REMOTE SENSING FOR FLOOD INUNDATION MAPPING USING VARIOUS PROCESSING METHODS WITH SENTINEL-1 AND SENTINEL-2

E. Stoyanova[1*]

[1]University of Architecture, Civil Engineering and Geodesy (UACEG), Faculty of Geodesy, Dept. of Photogrammetry and Cartography, Sofia, Bulgaria – stoyanova.elia@gmail.com

KEY WORDS: Sentinel-1, Sentinel-2, spectral indices, SAR, flood mapping, change detection

ABSTRACT:

The following paper discusses different remote sensing methodologies for flood mapping. The chosen study area is nearby Karlovo, Bulgaria where torrential rains in August and September 2022 caused devastating damages in the area. The location is still under critical status and damages are not completely evaluated, yet.
The aim of this study is to investigate how open satellite data can be applied in the mapping the results from the floods. The research team worked with radar and optical data from Sentinel-1 and Sentinel-2. Different technological approaches were applied to classify the land cover changes. Given the fact that the flood mass consisted mainly of mud an innovative approach was considered in order for the damages area to be computed.
Climate change predictions and deforestation suggest increasingly frequent floods in the future. For these reasons, rapid and timely flood mapping under specific conditions is very important in flood modelling, hazard and risk analysis. In order to investigate the flooded area in the region of the selected study area, different post-processing methods were used. The research team focused on using satellite imagery from both Sentinel-1 and Sentinel-2. Various spectral indices were computed as well as unsupervised and supervised classifications were applied. The results of the study were presented in the form of statistical analyses and comparison between the computational methods.

1. INTRODUCTION

A flood is a natural disaster in which a land area is temporarily flooded with a huge amount of water. It is obtained as a result of an increase in the level of water basins and riverbeds. The reasons for this are different, and most often these are intense rainfall, snowmelt, dam wall failure, soil erosion, human activity and others. Flooding can occur very slowly or occur in a matter of minutes.

They are also some of the most catastrophic natural disasters, as they cause significant damage to settlements, buildings, cars, bridges, roads and transport infrastructure. According to the Organization for Economic Co-operation and Development, floods cause more than $40 billion in damage worldwide annually. Millions of people and animals around the world are affected by floods every year, unfortunately sometimes losing their lives, with the number of deaths increasing in recent decades to over 100 people per year.

Often the worst part is not the flood itself, but the time after it. After the waters recede, the affected areas remain covered with mud and silt. Drinking water and the environment are contaminated with pesticides, various debris, fuel and untreated sewage. And in structures soaked with water, mold often forms, which can be very dangerous. Other problems for people after the floods include a lack of electricity and clean drinking water, which in turn can lead to disease outbreaks from the unsanitary conditions.

Precisely for these reasons, accurate and timely information about the size of the affected territory is needed. In this way, the damage will be able to be calculated and mapped, which will help with crisis management and recovery processes. This information is important because there is often a lack of timely, up-to-date and publicly available data on flood damage.

On August 22, 2022 the municipality of Karlovo declares a partial state of emergency due to heavy rains, as a large part of the streets and buildings are flooded. The amount of rain that fell is many times more than the monthly rainfall, but the nearby river did not overflow and people managed to cope without major damage. But the rains do not stop and on September 2, 2022, the dyke of the Stryama River broke and flooded several villages in the municipality of Karlovo, with the worst affected being the village of Bogdan and the village of Karavelovo, which are the subject of this study (Figure 1).

Figure 1. Location of case study: Bogdan and Karavelovo, Karlovo municipality, Bulgaria

The study is focused on the use of SNAP (Sentinel Application Platform), QGIS, Google Earth Pro and The Copernicus Open Access Hub. This contributes to the application of these studies by a wide range of interested specialists, as open access can accelerate getting good things done, helping spread the value more widely and reducing costs yet improving innovation.

2. STUDY AREA AND DATASET

2.1 Study area

As mentioned, the study focused mainly on two villages - Bogdan and Karavelovo in Karlovo municipality. They were chosen because the flood that hit them was one of the biggest disasters of 2022 in Bulgaria (Figure 2). The level of the river that floods the villages has risen by 3 meters in 8 hours, and the amount of rain that has fallen is over 250 litres per square meter.

Figure 2. The damage caused by the flood after September 2, 2022. Karavelovo village the day after the flood (*top left*); Multiple cars swept away in affected areas *(top right*); Home in the village of Karavelovo, it can be clearly seen how far the mud has reached (*bottom left*); The stadium of the village of Karavelovo covered with trees brought down from the river (*bottom right*). © Анастас Търпанов/ Anastas Turpanov (credit:https://www.dnevnik.bg/photos/2022/09/07/4388097_fotogaleriia_sled_potopa/ – accessed on 21 February 2023.)

The affected area is smaller in size. This is precisely why the research aims to explore the possibilities for remote sensing of smaller areas based on satellite images from the Copernicus program.

2.2 Dataset

For this paper, images from the Sentinel-1 and Sentinel-2 are used. They are provided free of charge by ESA as part of the Copernicus program. All images used in the study were obtained through the Copernicus Open Access Hub.

Two Sentinel-1A SAR datasets were used in the study. The first image was recorded before the heavy rains started and the river overflowed. The second image was recorded days after the floods. The main specifications of the datasets are presented in Table 1.

Mission	Date	Format-Mode	Polarization	More Information
Sentinel-1A	13 August 2022	GRD-IW	VV+VH	before the flood
Sentinel-1A	06 September 2022	GRD-IW	VV+VH	after the flood

Table 1. Specifications of Sentinel-1 images

A total of 3 multispectral images from Sentinel-2 were used. The first image was taken again before the heavy rains started and the river overflowed. The second image was again taken days after the floods. And the third was made 4 months after the disaster, the purpose of which is to see what the condition of the affected territory is. The main features of the images are presented in Table 2.

Mission	Date	Type	More Information
Sentinel-2A	18 August 2022	S2MSI2A	before the flood
Sentinel-2A	07 September 2022	S2MSI2A	after the flood
Sentinel-2B	08 January 2023	S2MSI2A	after the flood

Table 2. Specifications of Sentinel-2 images

Each of the 3 images consists of 13 bands and the features with their names, resolutions, bandwidths and central wavelengths are presented in Table 3 (Sentinel-2 User Handbook, 2015).

Sentinel-2 Bands	Central wavelength (nm)	Bandwidth (nm)	Resolution (m)
Band 1 - Coastal aerosol	443	20	60
Band 2 - Blue	490	65	10
Band 3 - Green	560	35	10
Band 4 - Red	665	30	10
Band 5 - Vegetation Red Edge	705	15	20
Band 6 - Vegetation Red Edge	740	15	20
Band 7 - Vegetation Red Edge	783	20	20
Band 8 - NIR	842	115	10
Band 8A - Vegetation Red Edge	865	20	20
Band 9 - Water vapour	945	20	60
Band 10 - SWIR - Cirrus	1375	30	60
Band 11 - SWIR	1610	90	20
Band 12 - SWIR	2190	180	20

Table 3. Features of Sentinel-2 images

3. METHODS

3.1 Sentinel-1 SAR data

To begin the practical part, the two Sentinel-1 SAR images were used. The processing was carried out according to the methodology specified in TRAINING KIT HAZA01 of RUS Copernicus.

Since the Area of Interest (AOI) is quite small and there is no need to process the whole image, subsets are made. Figure 3 shows the area covered by the study. Since the orbit state vectors provided in SAR product metadata are usually not exact, a precise exact orbit is applied. The orbital file provides accurate information about the satellite's position and velocity. Based on this information, the orbit state vectors in the abstract product metadata are updated. (SNAP Help)

Figure 3. Area of Interest for Sentinel-1 images

The next stage of processing is to remove the thermal noise. It is the background energy that is generated by the receiver itself. It skews the radar reflectivity to towards higher values and hampers the precision of radar reflectivity estimates. Level-1 products provide a noise LUT for each measurement dataset, provided in linear power, which can be used to remove the noise from the product (TRAINING KIT HAZA01).

The next step is calibration. The objective is to provide imagery in which the pixel values can be directly related to the radar backscatter of the scene. Though uncalibrated SAR imagery is sufficient for qualitative use, calibrated SAR images are essential to quantitative use of SAR data. The radiometric correction is also necessary for the comparison of SAR images acquired with different sensors, or acquired from the same sensor but at different times, in different modes, or processed by different processors. (SNAP Help)

Speckle Filtering is performed since SAR images have speckles which degrade the quality of the image and make interpretation of features more difficult (Figure 4). They are caused by random constructive and destructive interference of the de-phased but coherent return waves scattered by the elementary scatters within each resolution cell. (SNAP Help)

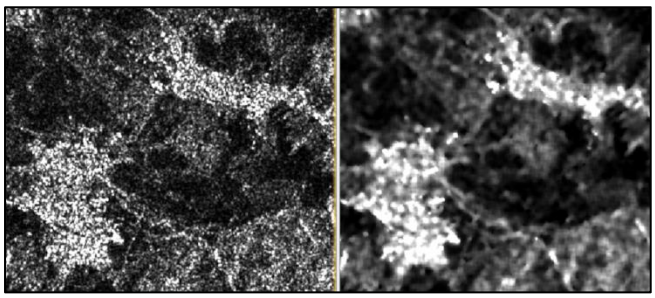

Figure 4. Speckle Filtering. View of the two villages before filtration (*left*), View after filtration (*right*).

The same threshold was chosen for both images so that the water could be separated from the other objects in the environment. The filtered backscatter coefficient histogram is used, where low values correspond to water and high values to other non-water objects. By using the color manipulation methods, the water is visualized in black, and the rest of the objects in the white-gray color range.

Topographic variations in the scene and tilt of the satellite sensor can lead to distortions of distances in SAR images. The Range Doppler orthorectification method for geocoding SAR images from single 2D raster radar geometry was used. It uses available orbit state vector information in the metadata, the radar timing annotations, the slant to ground range conversion parameters together with the reference DEM data to derive the precise geolocation information (SNAP Help). Terrain correction is used to compensate for these distortions and make the image as close as possible to its real appearance.

In both images, the two water bodies (red boxes, Figure 5) can be clearly seen. But no other indications of flooded areas are observed. Even before the flood occurs, there are more areas that can be identified as flooded. The blue arrows in Figure 5 show the areas that have undergone changes since the disaster. It is there that the river passes, leaving its bed and flooding the surrounding areas with mud.

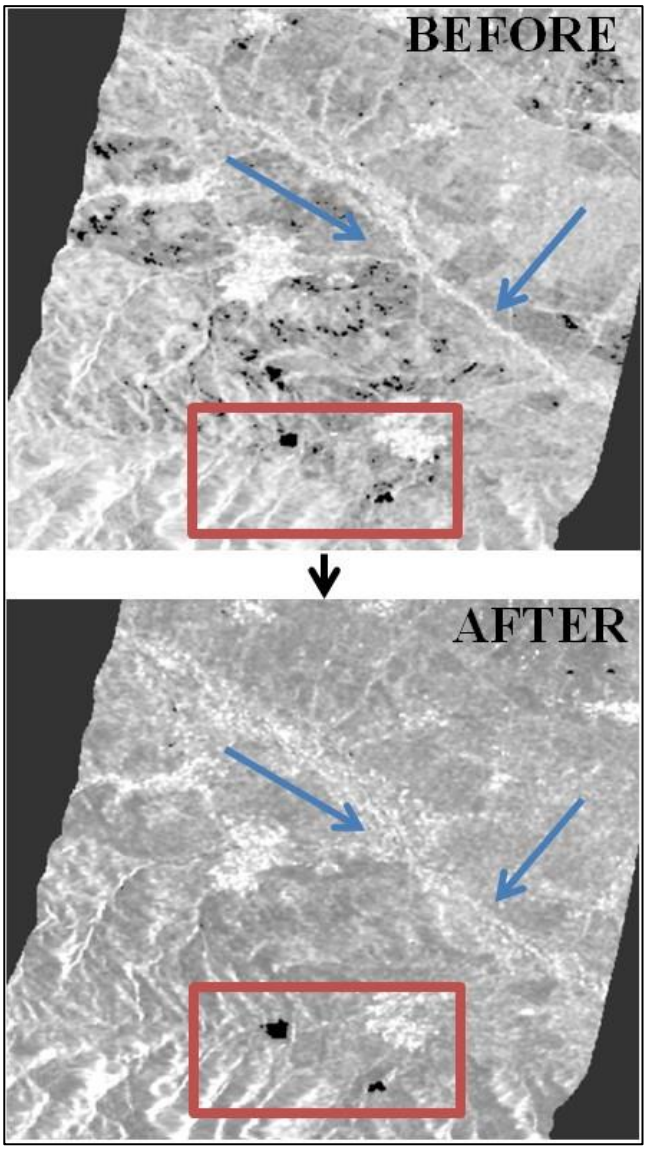

Figure 5. Results of radar data processing. Affected area before the flood (*top*), affected area after the flood (*bottom*).

So changes are observed after the processing, but since the flood mainly consists of mud, this type of treatment does not give the desired results to determine the affected area.

3.2 Sentinel-2 Optical data

Two different approaches were used in processing the optical data. One applied vegetation indices and the other emphasized supervised and unsupervised classification.

Because the same optical images from Sentinel-2 are used in both methods, the initial processing steps are identical. Processing begins with the creation of subsets, since the area of interest covers a significantly smaller area than that in the available images. This operation is applied to all three images using the same coordinate values of the endpoints of the geographic polygon (Figure 6).

Used satellite images are multi-size product since their bands are of different resolutions. The essence of processing begins with resampling the multi-size product to a single-size product. In these cases B2 band is used as reference band since it has the

biggest resolution of 10m. All other nodes will be resampled to match it's size. "Nearest" is the chosen upsampling method where every pixel value in the output product is set to the nearest input pixel value.

Figure 6. Area of Interest for Sentinel-2 images

3.2.1 Vegetation indices

The method for establishing post-flood changes is based on the analysis of the chosen area of interest through differences in terrain reflectivity and the use of different types of vegetation indices. A total of four such indices were used - NDVI, NDMI, MSI and NDWI.

The Normalized Difference Vegetation Index (NDVI) is an indicator that uses the red and near-infrared spectral bands (Equation (1)). It is one of the most well-known and used vegetation indices and it is highly associated with vegetation content. High NDVI values correspond to areas that reflect more in the near-infrared spectrum. Higher reflectance in the near-infrared corresponds to denser and healthier vegetation (GU, 2019).

$$\mathrm{NDVI} = \frac{(\mathrm{NIR}-\mathrm{Red})}{(\mathrm{NIR}+\mathrm{Red})} = \frac{(\mathrm{B8}-\mathrm{B4})}{(\mathrm{B8}+\mathrm{B4})}, \quad (1)$$

where NIR = Near-infrared spectral band
Red = Red spectral band
B4 = Red band in Sentinel-2 image
B8 = NIR band in Sentinel-2 image

The post-flood image was subtracted from the pre-flood image to generate a new difference image to serve as a measure of absolute change between captured images (Equation (2)). In the new raster, higher values represent areas of greatest change (high flood severity) and low or negative numbers representing non-flooded areas.

$$\mathrm{dNDVI} = \mathrm{NDVI}_{\mathrm{pre}} - \mathrm{NDVI}_{\mathrm{post}}, \quad (2)$$

where dNDVI = Differenced Normalized Difference Vegetation Index
$\mathrm{NDVI}_{\mathrm{pre}}$ = NDVI applied to a pre-flood image
$\mathrm{NDVI}_{\mathrm{post}}$ = NDVI applied to a post-flood image

Figure 7 shows the results of the NDVI analysis. For better understanding, only the damaged/changed areas after the flood are depicted.

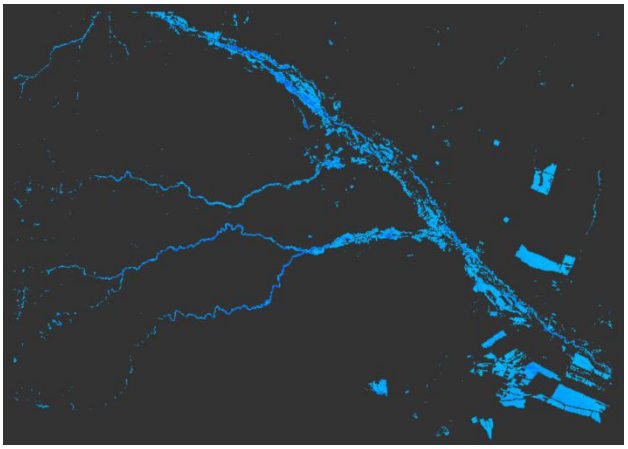

Figure 7. Flooded area according to NDVI

Normalized Difference Moisture Index (NDMI) is used to determine vegetation water content (Equation (3)). It is calculated as a ratio between the NIR and SWIR values (USGS, 2019). Generally higher value of NDMI specifies the presence of more soil moisture under massive aquatic bodies. Vegetation water content and soil moisture content are determined by it

$$\mathrm{NDMI} = \frac{(\mathrm{NIR}-\mathrm{SWIR})}{(\mathrm{NIR}+\mathrm{SWIR})} = \frac{(\mathrm{B8}-\mathrm{B11})}{(\mathrm{B8}+11)}, \quad (3)$$

where NIR = Near-infrared spectral band
SWIR = Short-wave infrared spectral band
B8 = NIR band in Sentinel-2 image
B11 = SWIR band in Sentinel-2 image

The same processing method was used after obtaining the results of this index. The post-flood image was subtracted from the pre-flood image to generate a new difference image to serve as a measure of absolute change between captured images (Equation (4)).

$$\mathrm{dNDMI} = \mathrm{NDMI}_{\mathrm{pre}} - \mathrm{NDMI}_{\mathrm{post}}, \quad (4)$$

where dNDMI = Differenced Normalized Difference Moisture Index
$\mathrm{NDMI}_{\mathrm{pre}}$ = NDMI applied to a pre-flood image
$\mathrm{NDMI}_{\mathrm{post}}$ = NDMI applied to a post-flood image

Figure 8 presents the results of the NDMI analysis. For better understanding, only the damaged/changed areas after the flood are depicted.

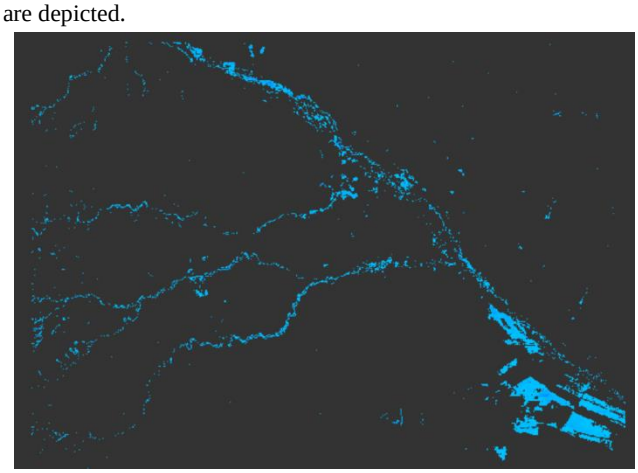

Figure 8. Flooded area according to NDMI

Moisture Stress Index (MSI) is used for canopy stress analysis, productivity prediction and biophysical modeling (Equation (5)). Interpretation of the MSI is inverted relative to other water vegetation indices. Higher values of the index indicate greater plant water stress and in inference, less soil moisture content (Welikhe et al., 2017).

$$\mathrm{MSI} = \frac{\mathrm{SWIR}}{\mathrm{NIR}} = \frac{\mathrm{B11}}{\mathrm{B8}}, \quad (5)$$

where NIR = Near-infrared spectral band
SWIR = Short-wave infrared spectral band
B8 = NIR band in Sentinel-2 image
B11 = SWIR band in Sentinel-2 image

Again after obtaining the results of this index the post-flood image was subtracted from the pre-flood image to generate a new difference image to serve as a measure of absolute change between captured images (Equation (6)).

$$\mathrm{dMSI} = \mathrm{MSI}_{\mathrm{pre}} - \mathrm{MSI}_{\mathrm{post}}, \quad (6)$$

where dMSI = Differenced Moisture Stress Index
$\mathrm{MSI}_{\mathrm{pre}}$ = MSI applied to a pre-flood image
$\mathrm{MSI}_{\mathrm{post}}$ = MSI applied to a post-flood image

Figure 9 shows the results of the MSI analysis. For better understanding, only the damaged/changed areas after the flood are depicted.

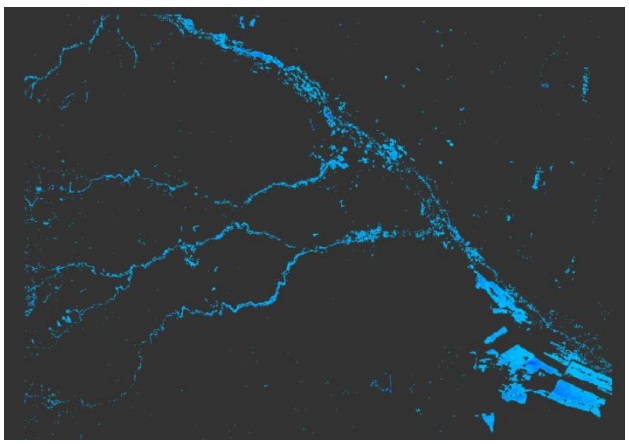

Figure 9. Flooded area according to MSI

Normalize Difference Water Index (NDWI) is used for the water bodies analysis. The index uses Green and Near-infrared bands and can enhance water information efficiently in most cases (Equation (7)). It is sensitive to build-up land and result in over-estimated water bodies (Bahadur, 2018).

$$\mathrm{NDWI} = \frac{(\mathrm{Green}-\mathrm{NIR})}{(\mathrm{Green}+\mathrm{NIR})} = \frac{(\mathrm{B3}-\mathrm{B8})}{(\mathrm{B3}+\mathrm{B8})}, \quad (7)$$

where NIR = Near-infrared spectral band
Green = Green spectral band
B8 = NIR band in Sentinel-2 image
B3 = Green band in Sentinel-2 image

Again the above mentioned option was used where the post-flood image was subtracted from the pre-flood image to generate a new difference image to serve as a measure of absolute change between captured images (Equation (8)).

$$\mathrm{dNDWI} = \mathrm{NDWI}_{\mathrm{pre}} - \mathrm{NDWI}_{\mathrm{post}}, \quad (8)$$

where dNDWI = Differenced Normalized Difference Water Index
$\mathrm{NDWI}_{\mathrm{pre}}$ = NDWI applied to a pre-flood image
$\mathrm{NDWI}_{\mathrm{post}}$ = NDWI applied to a post-flood image

Figure 10 presents the results of NDWI processing. For better understanding, only the damaged/altered areas after the flood are depicted.

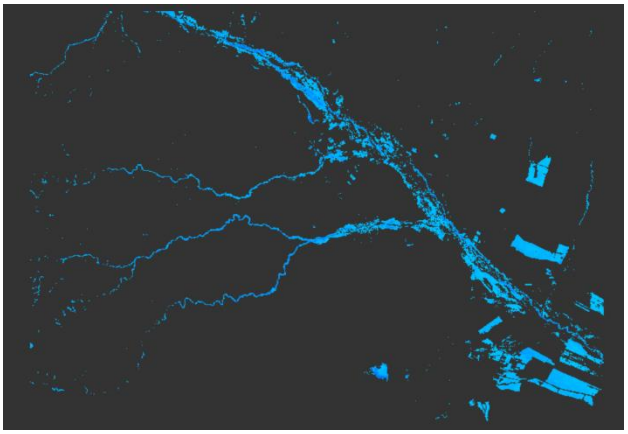

Figure 10. Flooded area according to NDWI

3.2.2 Classification methods

In order to make better use of the information contained in the spectral zones, procedures based on developed algorithms and recognizing spectral homogeneity are used. Classifications of multispectral Sentinel-2 images obtained from the real world are used to identify the individual land cover elements. Through the classifications used, different classes are recognized on the selected image based on its spectral characteristics.

Classifications are divided into two types:
- Unsupervised – in learning mode, they are automatic and do not depend on the knowledge of terrain data and do not require additional information on the assignment of pixels to the reduced classes.
- Supervised – in self-learning mode, they are semi-automatic and more accurate compared to unsupervised classes. They require prior knowledge of the classes for a sufficient number of pixels to be recognized by the analyzer, or a field search to be performed.

For each of these types, one method is applied - K-Means (KM) Cluster Analysis and Maximum Likelihood Classification.

K-Means Cluster Analysis /Unsupervised classification/ is the classification of objects into different groups, or more precisely, the division of a data set into clusters so that the data in each share some common feature - often proximity according to a certain distance measure (Filipova, 2020). Data clustering is a common statistical data analysis technique that is used in many fields, including machine learning, data mining, pattern recognition, image analysis, and bioinformatics. In this particular case, 6 clusters and 30 iterations were selected as parameters of this classification. Figure 11 presents the classification by this method and more information about the obtained results.

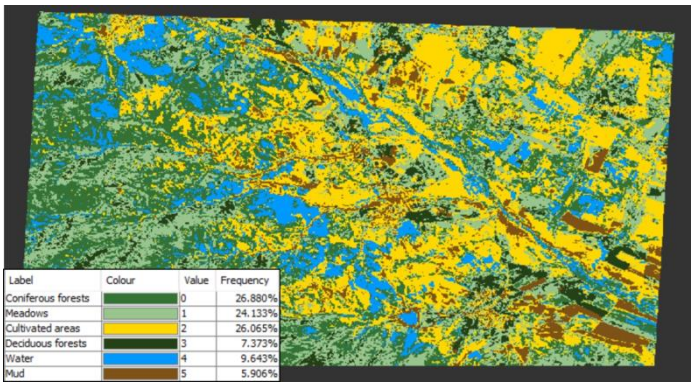

Figure 11. K-Means Cluster Analysis

The **Maximum likelihood classifier** /Supervised classification/ is one of the most popular classification methods, in which a pixel with the maximum likelihood is classified into the corresponding class. The likelihood is defined as the posterior probability of a pixel belonging to a given class (SNAP Help). A total of 6 vector data containers were created, and a different number of standards were added to them, corresponding to different objects of the terrain cover: coniferous forests, deciduous forests, meadows, water, mud and cultivated areas. Figure 12 presents the classification by this method and more information about the obtained results.

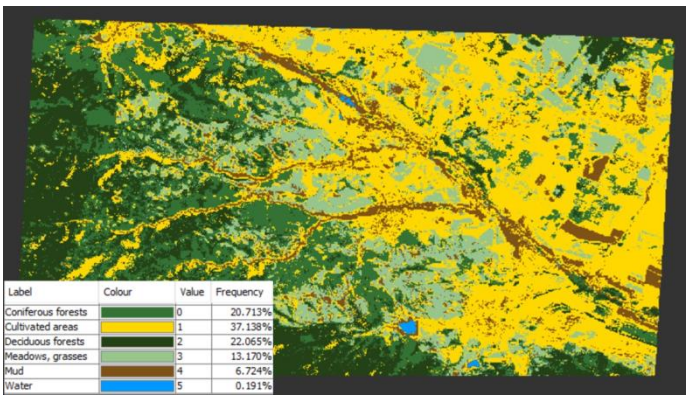

Figure 12. Maximum likelihood classifier

3.2.3 What happens after 4 months?

To understand what happens to the affected territory a few months later, an image from Sentinel-2 from January 8, 2023 was used. For this purpose, only visual interpretation was done. No vegetation indices or classifications were used, as trees and plants are already at a different stage of their phenological cycle and the results would not be comparable, which could lead to misinterpretation of the results.

Figure 13 presents images of the village of Karavelovo before and after the flood, as well as four months after it. The mud deposits that have been brought down from the river can be clearly seen. In the second series of photos, it can be established what the situation is now. It can be seen that almost all the mud is still there and that only a small part of the centre of the village has been cleaned.

Figure 13. Karavelovo village. Photo from August 18, 2022 before the flood (*top left*); Photo from September 7, 2022 after the flood (*top right and bottom left*); photo from January 8, 2023 - 4 months after the disaster (*bottom right*).

4. RESULTS

Visually, the results of processing the SAR images from Sentinel-1 are presented in Figure 5. All the water bodies /dams/ are well represented, but since the flood mainly consists of mud, the change before and after the disaster cannot be established in good quality and quantity.

The results of the processing based on the vegetation indices are shown in Figures 7 to 10. They visualize the affected flooded areas more clearly. Figure 13 presents a visual comparison of the four indices. It can be seen that the best results are given by NDVI and NDWI, since they have few residual pixels that do not carry qualitative information for interpreting the results. Also, with these indices, the more strongly affected territories are distinguished clearly and densely with well-defined contours.

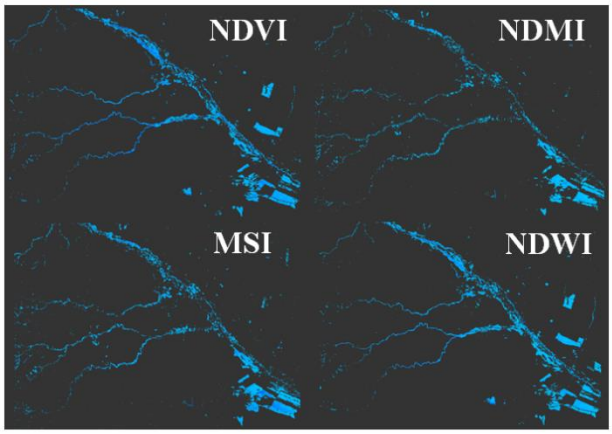

Figure 14. Comparison of flooded areas calculated from vegetation indices

The final processing products of the classification methods are shown in Figures 11 and 12, where it is obvious that the one in the training mode /Maximum likelihood classifier/ gave better results. While processing by the method without training /K-Means Cluster Analysis/ has given too many water areas. The results of the quantitative evaluation by the two optical methods of processing are presented in Table 4.

Method	Name	Flooded area [km^2]
Vegetation indicies	NDVI	8.431
	NDMI	5.336
	MSI	7.446
	NDWI	8.586
Unsupervised classification	K-Means Cluster Analysis	9.888
Supervised classification	Maximum likelihood classifier	11.178

Table 4. Size of the flooded area obtained by the different methods

5. CONCLUSION

The specifics of this case study include free-to-use images from the Copernicus program, the use of different methodologies, a small affected area, an urbanized and forested area, and a flood mainly consisting of mud. Based on the obtained results of the processing by the different methods and subsequent visual interpretation, it was found that for this case the best results are obtained by using two of the vegetation indices Normalize Difference Water Index and Normalized Difference Vegetation Index. With them, the results are best visible, the processing time is short and fast, and an affected area can be easily calculated in a desired projection.
Acceptable results are obtained with supervised classification, but there the assigned classes also have a great influence. Errors can be obtained by setting these benchmarks incorrectly. The worst results are observed when using SAR images, because the affected area is not very large, and in addition, the main part of the flood consists of mud.

According to the Bulgaria's Flood Risk Management Plans, so far the affected areas have not been identified as areas of significant potential high or medium flood risk. The results obtained from the research would support the future analyses related to this risk for the future periods.

Since the post-flood situation is not yet fully under control, the results can easily be integrated into a geographic information system and used by a wide range of specialists. This can facilitate the faster implementation of activities related to the restoration of normal life in populated areas and the reduction of damage after the disaster.

Figure 15 presents the flood affected areas obtained from NDVI results and visualized in Google Earth Pro.

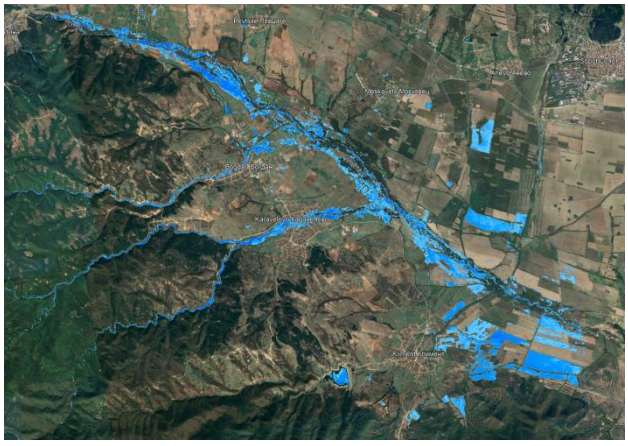

Figure 15. Flooded areas

The timely use of remote and other flood monitoring methods is extremely important. But it would be best if such disasters did not happen at all. Therefore, in order to limit the risk of floods, the Ministry of the Interior of the Republic of Bulgaria advises:

- Each person should become aware of the risk of flooding for the locality in which he lives or works;
- Each person should know about the nearest safe place, the shortest and safest route to evacuate;
- Do not throw construction and household waste into the riverbeds, this reduces the conductivity of the riverbed;
- Do not block river currents for the purpose of taking water for watering or bathing animals, as these barriers multiply the destructive power of water during floods;
- Not to destroy and pierce the dams of the rivers for the purpose of taking water for irrigation or other activities;
- To report to the local municipality, town hall or regional administration, if the riverbed and the spaces under the bridges are not cleaned of waste, construction materials, trees and others;
- Do not build residential and agricultural buildings and other structures in unprotected river floodplains.

REFERENCES

Anusha, N. , Bharathi, B., 2019: Flood detection and flood mapping using multi-temporal synthetic aperture radar and optical data. The Egyptian Journal of Remote Sensing and Space Science, Volume 23, Issue 2, August 2020, Pages 207-219. https://doi.org/10.1016/j.ejrs.2019.01.001.

Bhangale, U., More, S., Shaikh, T., Patil S., More, N., 2020: Analysis of Surface Water Resources Using Sentinel-2 Imagery. Procedia Computer Science 171 (2020) 2645–2654.

Bhattacharya, S., Halder, S., Nag, S., Roy, P., Roy, M., 2021; Advances in Water Resources Management for Sustainable Use, DOI: 10.1007/978-981-33-6412-7_18.

Elhag, M., Bahrawi, J., 2016: Soil Salinity Mapping and Hydrological Drought Indices Assessment in Arid Environments Based on Remote Sensing Techniques. Geosci. Instrum. Method. Data Syst. Discuss., doi:10.5194/gi-2016-39.

Filipova S., Filipov D., Raeva P., SUSTAINABLE MANAGEMENT OF WATER BODIES BASED ON MULTITEMPORAL SATELLITE IMAGES, Proceedings Vol. 1, 8th International Conference on Cartography and GIS, 2020, Nessebar, Bulgaria ISSN: 1314-0604, pp. 693-701

Foroughnia, F.; Alfieri, S.M.; Menenti, M.; Lindenbergh, R. Evaluation of SAR and Optical Data for Flood Delineation Using Supervised and Unsupervised Classification. Remote Sens. 2022, 14, 3718. https://doi.org/10.3390/rs14153718.

Gilabert, M., Gonzalez-Piqueras, J., Martinez, B., 2011: Theory and application of vegetation indices. Remote Sensing Optical Observations of Vegetation Properties, 2010: 1- 43, ISBN: 9/8-87 -308-0421-7.

Güvela, Ş., Akgül, M., Aksu, H., Flood inundation maps using Sentinel-2: a case study in Berdan Plain. Water Supply Vol 22 No 4, 4098 doi: 10.2166/ws.2022.039.

https://giscrack.com/list-of-spectral-indices-for-sentinel-and-landsat/

https://www.mvr.bg/gdpbzn/info-center/pravila-povedenie/pri-navodnenia

https://www.nationalgeographic.com/environment/article/floods

https://pro.arcgis.com/en/pro-app/latest/help/data/imagery/indices-gallery.htm

https://scihub.copernicus.eu/

https://www.usgs.gov/landsat-missions/landsat-normalized-difference-vegetation-index

Kamenova, K., Dimitrov, P. 2020: Evaluation of Sentinel-2 vegetation indices for prediction of LAI, fAPAR and fCover of winter wheat in Bulgaria. European Journal of Remote Sensing. DOI: 10.1080/22797254.2020.1839359.

Kriegler, F.J., Malila, W.A., Nalepka, R.F. and Richardson, W., 1969, Preprocessing transformations and their effect on multispectral recognition, in: Proceedings of the sixth International Symposium on Remote Sensing of Environment, University of Michigan, Ann Arbor, MI, pp. 97-131

Marinova, S., Thematic Mapping and Visualization for Early Warning and Crisis Management, UACEG, Sofia, 2018, pp. 154, ISBN 978-954-724-108-4.

McKenna, P., Phinn, S., Erskine, P., 2018: Fire Severity and Vegetation Recovery on Mine Site Rehabilitation Using WorldView-3 Imagery. Fire 2018, 1, 22; doi:10.3390/fire1020022.

Medina1, J., Blanco, A., Candido, C., 2020: Land cover monitoring of Laguna lake watershed using MODIS NDVI data. The International Archives of the Photogrammetry, Remote Sensing and Spatial Information Sciences, Volume XLII-3/W11.

Meyer, R., Søgaard, M., Schødt, M., Horion, S., Prishchepov, A. 2022: Emergency flood mapping in Australia with Sentinel-1 and Sentinel-2 satellite imagery. BSGLg, 78, 2022, 123-138. https://doi.org/10.25518/0770-7576.6653.

Na Sun, Cailin Li, Baoyun Guo, Xiaokai Sun, Yukai Yao, Yue Wang, 2022: Research status and development trend of photogrammetry and remote sensing in urban flood disasters. ISPRS Annals of the Photogrammetry, Remote Sensing and Spatial Information Sciences, Volume X-3/W1-2022

Nhangumbe, M., Nascetti, A., Ban, Y. 2023: Multi-Temporal Sentinel-1 SAR and Sentinel-2 MSI Data for Flood Mapping and Damage Assessment in Mozambique. ISPRS Int. J. Geo-Inf. 2023, 12, 53. https://doi.org/10.3390/ijgi12020053.

RUS-Copernicus. Training Kit - HAZA01 - Flood monitoring with Sentinel-1 using s-1 toolbox – January 2015, MALAWI.

SNAP Help

Sentinel-1 SAR User Guide

Sentinel-2 User Handbook, ESA. 2015

Tarpanelli, A., Mondini, A., Camici, S., 2022: Effectiveness of Sentinel-1 and Sentinel-2 for flood detection assessment in Europe. Nat. Hazards Earth Syst. Sci., 22, 2473–2489, 2022 https://doi.org/10.5194/nhess-22-2473-2022.

Tavus, B., Kocaman, S., Nefeslioglu, H., Gokceoglu, C., 2020: A fusion approach for flood mapping using SENTINEL-1 and SENTINEL-2 datasets. The International Archives of the Photogrammetry, Remote Sensing and Spatial Information Sciences, Volume XLIII-B3-2020,https://doi.org/10.5194/isprs-archives-XLIII-B3-2020-641-2020.

Tavus, B., Kocaman, S., Nefeslioglu, H.A., Gokceoglu, C., 2019: FLOOD MAPPING USING SENTINEL-1 SAR DATA: A CASE STUDY OF ORDU 8 AUGUST 2018 FLOOD. International Journal of Environment and Geoinformatics 6(3):333-337. http://dx.doi.org/10.30897/ijegeo.666212.

Welikhe, P., Quansah, JE., Fall, S., Elhenney, WMc., 2017; Estimation of Soil Moisture Percentage Using LANDSAT-based Moisture Stress, Index. J Remote Sensing & GIS 6: 200. doi: 10.4172/2469-4134.1000200.

Zhang, M., Chen, F., Liang, D., Tian, B., Yang, A., 2020: Use of Sentinel-1 GRD SAR Images to Delineate Flood Extent in Pakistan. Sustainability 2020, 12(14), 5784; https://doi.org/10.3390/su12145784.